**Power Electronic Systems
Laboratory**

Optimal Design of LCL Harmonic Filters for Three-Phase PFC Rectifiers

J. Mühlethaler
M. Schweizer
R. Blattmann
J. W. Kolar
A. Ecklebe

ETH

Eidgenössische Technische Hochschule Zürich
Swiss Federal Institute of Technology Zurich

Optimal Design of LCL Harmonic Filters for Three-Phase PFC Rectifiers

J. Mühlethaler*, M. Schweizer*, R. Blattmann*, J. W. Kolar*, and A. Ecklebe†

*Power Electronic Systems Laboratory, ETH Zurich, Email: muehlethaler@lem.ee.ethz.ch

†ABB Switzerland Ltd., Corporate Research, CH-5405 Baden-Dättwil

Abstract—**Inductive components such as line filter inductors or transformers occupy a significant amount of space in today's power electronic systems, and furthermore, considerable losses occur in these components. A main application of filter inductors are EMI filters, as e.g. employed for the attenuation of switching frequency harmonics of PFC rectifier systems. In this paper a design procedure for the mains side LCL filter of an active three-phase rectifier is introduced. The procedure is based on a generic optimization approach, which guarantees a low volume and/or low losses. Different designs are calculated to show the trade-off between filter volume and filter losses. The design procedure is verified by experimental measurements.**

I. Introduction

The trend in power electronics research is towards higher efficiency and higher power density of converter systems. This trend is driven by cost considerations, e.g. material economies, space limitations, e.g. for automotive applications, and increasing efficiency requirements, e.g. for telecom applications. The increase of the power density often affects the efficiency, i.e. a trade-off between these two quality indices exists [1].

Inductive components occupy a significant amount of space in today's power electronic systems, and furthermore, considerable losses occur in these components. Therefore, in order to increase the power density and/or efficiency of power electronic systems, losses in inductive components must be reduced, and/or new cooling concepts need to be investigated.

At the Power Electronic Systems Laboratory at ETH Zurich a project has been initiated with the goal to establish comprehensive models of inductive power components which can be adapted to various geometric properties, operating conditions and cooling conditions. These models will form the basis for the optimization of inductive components employed in key power electronics applications. The aim of this paper is to use these previously derived models to design LCL input filters of a three-phase Power Factor Correction (PFC) rectifier.

LCL input filters are an attractive solution to attenuate switching frequency current harmonics of active voltage source rectifiers [2], [3]. In this work a design procedure for LCL filters based on a generic optimization approach is introduced guaranteeing low volume and/or low losses. Different designs are calculated showing the trade-off between filter volume and filter losses.

In Section II the three-phase PFC rectifier is introduced, in Section III the applied models of the LCL filter components are discussed, and in Section IV the optimization algorithm is described. Simulation and experimental results are given in Sections V and VI respectively.

II. Three-Phase PFC Rectifier with Input Filter

The three-phase PFC rectifier investigated in this work is shown in Fig. 1. The rectifier comprises in each phase a boost inductor L_2, a damped LC filter $L_1/C/C_{\mathrm{d}}/R_{\mathrm{d}}$ and a pair of switches with free-wheeling diodes. The load is assumed to be a DC current source. The considered operating point of the PFC rectifier is described in Table I. A Space Vector Modulation (SVM) scheme with loss-optimal clamping has been implemented to have a fundamental displacement factor of $\cos \phi = 1$. The functionality and the detailed control of the used SVM scheme are described in [4]. The three-phase PFC rectifier with input filter has been simulated in MATLAB/Simulink, where the non-linearity of the core material of the inductors, i.e. the change of the inductance value with changing current, is taken into account.

The three inductors $L_{1,\mathrm{a}}$, $L_{1,\mathrm{b}}$, and $L_{1,\mathrm{c}}$, and the three capacitors C_{a}, C_{b}, and C_{c} in star arrangement, together with the three boost inductors $L_{2,\mathrm{a}}$, $L_{2,\mathrm{b}}$ and $L_{2,\mathrm{c}}$, result in a third order LCL low pass filter between the mains and the switching stage. The capacitor/resistor branches $C_{\mathrm{d,a}}/R_{\mathrm{d,a}}$, $C_{\mathrm{d,b}}/R_{\mathrm{d,b}}$, and $C_{\mathrm{d,c}}/R_{\mathrm{d,c}}$ are necessary to damp the resonance of the LC input filter. All inductors are assumed to have the same geometry, which is illustrated in Fig. 1(b). The cores are made of grain-oriented steel (M165-35S). Solid copper wire is taken for the conductors. The windings are divided into two halves arranged on the two legs which leads to a more distributed winding structure. A more distributed winding structure has advantages such as better heat dissipation capabilities, lower inductor volume, etc.

III. Modeling of Input Filter Components

The loss modeling is based on the framework introduced in [5], where a high level of accuracy has been achieved by combining the best state-of-the-art approaches and by embedding newly-developed approaches into a novel loss calculation framework. In [5] the impact of the peak-to-peak flux density ΔB, frequency f, DC premagnetization H_{DC},
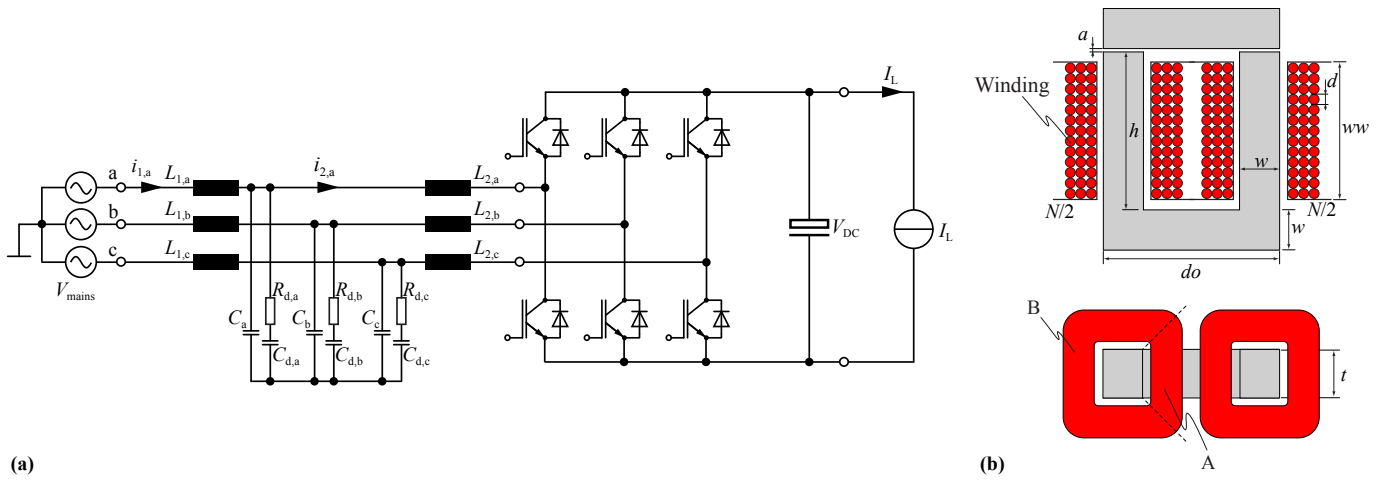
Fig. 1. (a) Three-phase PFC rectifier with LCL input filter. (b) Cross-sections of inductors employed in the input filter.

temperature T, core shape, minor and major BH-loops, flux waveform, and material on the core loss calculation has been considered. In order to calculate the winding losses, formulas for round conductors and litz wires, each considering skin- and proximity effects and also considering the influence of an air-gap fringing field have been included. In the following, a discussion about the implemented models for the employed inductors (cf. Fig. 1(b)) is given.

A. Calculation of the Inductance

The inductance of an inductive component with N winding turns and a total magnetic reluctance $R_{\mathrm{m,tot}}$ is calculated as

$$L = \frac{N^2}{R_{\mathrm{m,tot}}}. \tag{1}$$

Accordingly, the reluctance of each section of the flux path has to be derived first in order to calculate $R_{\mathrm{m,tot}}$. The total reluctance for a general inductor is calculated as a function of the core reluctances and air gap reluctances. The core and air gap reluctances can be determined applying the methods described in [6]. The reluctances of the core depend on the relative permeability μ_{r} which is defined by the (nonlinear) BH-relation of the core material, hence the reluctance is described as a function of the flux. Therefore, as the flux depends on the core reluctance and the reluctance depends on the flux, the system can only be solved iteratively by using a numerical method. In the case at hand, the problem has been solved by applying the Newton approach.

The reluctance model of the inductance of Fig. 1(b) consists of one voltage source (representing the two separated wind-ings), one air gap reluctance (representing the two air gaps) and one core reluctance. The fact that the flux density in core parts very close to the air gap is (slightly) reduced as the flux lines already left the core has been neglected.

B. Core Losses

The applied core loss approach is described in [5] in detail and can be seen as a hybrid of the *improved-improved Generalized Steinmetz Equation* i²GSE [7] and a loss map

approach: a loss map is experimentally determined and the interpolation and extrapolation for operating points in between the measured values is then made with the i²GSE.

The flux density waveform for which the losses have to be calculated is e.g. simulated in a circuit simulator, where the magnetic part is modeled as a reluctance model. This simulated waveform is then divided into its fundamental flux waveform and into piecewise linear flux waveform segments. The loss energy is then derived for the fundamental and all piecewise linear segments, summed-up and divided by the fundamental period length in order to determine the average core loss. The DC flux level of each piecewise linear flux segment is considered, as this influences the core losses [8]. Furthermore, the relaxation term of the i²GSE is evaluated for each transition from one piecewise linear flux segment to another.

Another aspect to be considered in the core loss calculation is the effect of the core shape/size. By introducing a reluc-tance model of the core, the flux density can be calculated. Subsequently, for each core section with (approximately) homogenous flux density, the losses can be determined. In the case at hand, the core has been divided into four straight core sections and four corner sections. The core losses of the sections are then summed-up to obtain the total core losses.

C. Winding Losses

The second source of losses in inductive components are the ohmic losses in the windings. The resistance of a conductor increases with increasing frequency due to eddy currents. Self-induced eddy currents inside a conductor lead to the skin effect. Eddy currents due to an external alternating magnetic field, e.g. the air gap fringing field or the magnetic field from other conductors, lead to the proximity effect.

The sum of the DC losses and the skin effect losses per unit length in round conductors (cf. Fig. 2(a)) can be calculated as [9]

$$P_{\mathrm{S}} = R_{\mathrm{DC}} \cdot F_{\mathrm{R}}(f) \cdot \hat{I}^2 \tag{2}$$
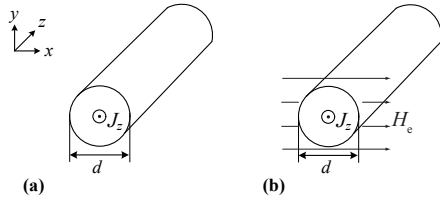
Fig. 2. Cross-section of the round conductor considered with a current in z-direction. The conductor is infinitely large in z-direction.

and[1]

$$F_{\mathrm{R}}(f) = \frac{\xi}{4\sqrt{2}} \left(\frac{\mathrm{ber}_0(\xi)\mathrm{bei}_1(\xi) - \mathrm{ber}_0(\xi)\mathrm{ber}_1(\xi)}{\mathrm{ber}_1(\xi)^2 + \mathrm{bei}_1(\xi)^2} \right. \\ \left. - \frac{\mathrm{bei}_0(\xi)\mathrm{ber}_1(\xi) + \mathrm{bei}_0(\xi)\mathrm{bei}_1(\xi)}{\mathrm{ber}_1(\xi)^2 + \mathrm{bei}_1(\xi)^2} \right), \quad (3)$$

with $\delta = \frac{1}{\sqrt{\pi \mu_0 \sigma f}}$, $\xi = \frac{d}{\sqrt{2}\delta}$, $R_{\mathrm{DC}} = \frac{4}{\sigma \pi d^2}$; δ is commonly named the skin depth, f is the frequency, d is the conductor diameter, and σ is the electric conductivity of the conductor material.

The proximity effect losses in round conductors (cf. Fig. 2(b)) per unit length can be calculated as [9]

$$P_{\mathrm{P}} = R_{\mathrm{DC}} \cdot G_{\mathrm{R}}(f) \cdot \hat{H}_{\mathrm{e}}^2 \quad (4)$$

and

$$G_{\mathrm{R}}(f) = -\frac{\xi \pi^2 d^2}{2\sqrt{2}} \left(\frac{\mathrm{ber}_2(\xi)\mathrm{ber}_1(\xi) + \mathrm{ber}_2(\xi)\mathrm{bei}_1(\xi)}{\mathrm{ber}_0(\xi)^2 + \mathrm{bei}_0(\xi)^2} \right. \\ \left. + \frac{\mathrm{bei}_2(\xi)\mathrm{bei}_1(\xi) - \mathrm{bei}_2(\xi)\mathrm{ber}_1(\xi)}{\mathrm{ber}_0(\xi)^2 + \mathrm{bei}_0(\xi)^2} \right). \quad (5)$$

R_{DC} is the resistance per unit length, hence the losses P_{S} and P_{P} are losses per unit length as well. The external magnetic field strength H_{e} of every conductor has to be known when calculating the proximity losses. In the case of an un-gapped core and windings that are fully-enclosed by core material, 1D approximations to derive the magnetic field exist. The most popular method is the Dowell method [11]. However, in the case of gapped cores, such 1D approximations are not applicable as the fringing field of the air gap cannot be described in a 1D manner. For the employed gapped cores another approach has to be selected. The applied approach is a 2D approach and described in detail in [5], where it has been implemented based on a previously presented work [12].

The magnetic field at any position can be derived as the superposition of the fields of each of the conductors. The impact of a magnetic conducting material can further be modeled with the *method of images*, where additional currents that are the mirrored version of the original currents are added to replace the magnetic material [12]. In case of windings that are fully-enclosed by magnetic material (i.e. in the core window), a new

---

[1]The solution for F_{R} (and G_{R}) is based on a *Bessel differential equation* that has the form $x^2 y'' + x y' + (k^2 x^2 - v^2)y = 0$. With the general solution $y = C_1 \mathbb{J}_v(kx) + C_2 \mathbb{Y}_v(kx)$, whereas $\mathbb{J}_v(kx)$ is known as *Bessel function of the first kind* and order v and $\mathbb{Y}_v(kx)$ is known as *Bessel function of the second kind* and order v [10]. Furthermore, to resolve $\mathbb{J}_v(kx)$ into its real- and imaginary part, the *Kelvin functions* can be used: $\mathbb{J}_v(\mathrm{j}^{\frac{3}{2}}x) = \mathrm{ber}_v x + \mathrm{j}\,\mathrm{bei}_v x$.
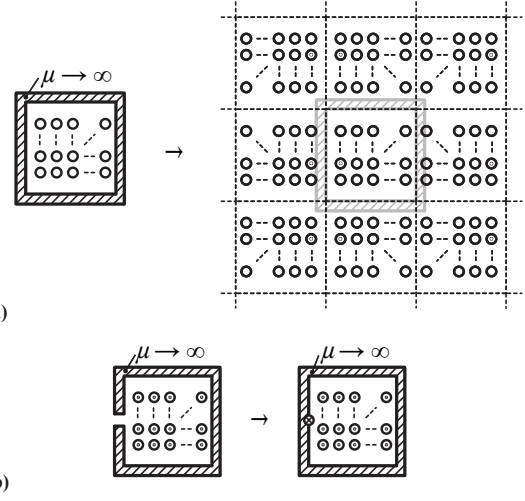

Fig. 3. (a) Illustration of the *method of images* (mirroring). (b) Illustration of modeling an air gap as a fictitious conductor.

wall is created at each mirroring step as the walls have to be mirrored as well. The mirroring can be continued to pushing the walls away. This is illustrated in Fig. 3(a). For this work, the mirroring has been stopped after the material was replaced by conductors three times in each direction. The presence of an air gap can be modeled as a fictitious conductor without eddy currents equal to the magneto-motive force (mmf) across the air gap [12] as illustrated in Fig. 3(b).

According to the above discussion the winding losses have to be calculated differently for the sections A and B illustrated in Fig. 1(b), as the mirroring leads to different magnetic fields.

D. Thermal Modeling

Fig. 4. Thermal model using only one thermal resistance.

A thermal model is important when minimizing the filter volume, as the maximum temperature allowed is the limiting factor when reducing volume. The model used in this work consists of only one thermal resistance R_{th} and is illustrated in Fig. 4. The inductor temperature T_{L} is assumed to be homogenous; it can be calculated as

$$T_{\mathrm{L}} = T_{\mathrm{A}} + P_{\mathrm{loss}} R_{\mathrm{th}}, \quad (6)$$

where P_{loss} are the total losses occurring in the inductor, consisting of core and winding losses, and T_{A} is the ambient temperature. The ambient temperature T_{A} is assumed to be constant at $25\,^\circ\mathrm{C}$.

The heat transfer due to convection is described with

$$P = \alpha A (T_{\mathrm{L}} - T_{\mathrm{A}}), \quad (7)$$

where P is the heat flow, A the surface area, T_{L} the body surface temperature (i.e. inductor temperature), and T_{A} the fluid (i.e. ambient air) temperature. α is a coefficient that

is determined by a set of characteristic dimensionless numbers, the Nusselt, Grashof, Prandtl, and Rayleigh numbers. Radiation has to be considered as a second important heat transfer mechanism and is described by the Stefan-Boltzmann law. Details about thermal modeling are not given here; the interested reader is referred to [13], from where the formulas used in this work have been taken.

E. Capacitor Modeling

The filter and damping capacitors are selected from the EPCOS X2 MKP film capacitors series; which have a rated voltage of $305\,\mathrm{V}$. The dissipation factor is specified as $\tan\delta \leq 1\,\mathrm{W/kvar}$ (at $1\,\mathrm{kHz}$) [14], which enables the capacitor loss calculation. The capacitance density to calculate the capacitors volume can be approximated with $0.18\,\mu\mathrm{F/cm^3}$. The capacitance density has been approximated by dividing the capacitance value of several components by the according component volume.

F. Damping Branch

An LC filter is added between the boost inductor and the mains to meet a THD constraint. The additional LC filter changes the dynamics of the converter and may even increase the current ripple at the filter resonant frequency. Therefore, a $C_\mathrm{d}/R_\mathrm{d}$ damping branch has been added for damping. In [15], [16] it is described how to optimally choose C_d and R_d. Basically, there is a trade-off between the size of damping capacitor C_d and the damping achieved. For this work, $C_\mathrm{d} = C$ has been selected as it showed to be a good compromise between additional volume needed and a reasonable damping achieved. The value of the damping resistance that leads to optimal damping is then [15], [16]

$$R_\mathrm{d} = \sqrt{2.1\frac{L_1}{C}}. \tag{8}$$

The $C_\mathrm{d}/R_\mathrm{d}$ damping branch increases the reactive power consumption of the PFC rectifier system. Therefore, often other damping structures, such as the R_f-L_b series damping structure, are selected [16]. For this work, however, the $C_\mathrm{d}/R_\mathrm{d}$ damping branch has been favored as its practical realization is easier and lower losses are expected. Furthermore, as will be seen in Section V, the reactive power consumption of the PFC rectifier system including the damped LC input filter is in the case at hand rather small.

IV. Optimization of the Input Filter

The aim of this paper is to optimally design a harmonic filter of the introduced three-phase PFC rectifier. For the evaluation of different filter structures, a cost function is defined that weights the filter losses and filter volume according to the designer needs. In the following, the steps towards an optimal design are described. All steps are illustrated in Fig. 6. The optimization constraints are discussed first.
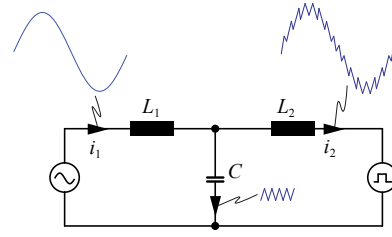

Fig. 5. Idealized current waveforms for each filter component.

A. Optimization Constraints and Conditions

The high-frequency ripple in the current $i_{2,a/b/c}$ is limited to the value $I_\mathrm{HF,pp,max}$, which is important as a too high $I_\mathrm{HF,pp,max}$ e.g. impairs controllability (for instance, an accurate current measurement becomes more difficult). Furthermore, the THD of the mains current should be limited to fulfill industrial norms. Two other design constraints are the maximum temperature T_max and the maximum volume V_max the filter is allowed to have. A fixed switching frequency f_sw is assumed. The DC link voltage V_DC and the load current I_L are also assumed to be given and constant. All constraints/condition values for the current system are given in Fig. 6.

B. Calculation of $L_{2,\mathrm{min}}$

The minimum value of inductance $L_{2,\mathrm{min}}$ can be calculated based on the constraint $I_\mathrm{HF,pp,max}$ as

$$L_{2,\mathrm{min}} = \frac{\sqrt{2}|V_\mathrm{mains}|}{V_\mathrm{DC}/\sqrt{3}}\cos(\pi/6)\cdot\frac{\frac{2}{3}V_\mathrm{DC}-\sqrt{2}V_\mathrm{mains}}{I_\mathrm{HF,pp,max}\cdot f_\mathrm{sw}}. \tag{9}$$

It can be shown that, in case of a fundamental displacement factor of $\cos\phi = 1$, the maximum current ripple $I_\mathrm{HF,pp,max}$ occurs when the current reaches the peak value $\hat{I}_\mathrm{LF}$ of the fundamental. This has further been confirmed by simulation results. As a consequence, the minimum value $L_{2,\mathrm{min}}$ has to be met at the current $\hat{I}_\mathrm{LF}$.

C. Loss Calculation of Filter Components

In the foregoing sections it has been shown how an accurate loss modeling based on simulated current and voltage waveforms is possible. However, such a calculation based on simulated waveforms is time consuming and therefore, for an efficient optimization, simplifications have to be made. In Fig. 5, idealized current waveforms for each filter component of a phase are illustrated. The current in L_1 is approximated as purely sinusoidal with a peak value of

$$\hat{I} = \frac{2}{3}\frac{I_\mathrm{L}V_\mathrm{DC}}{\sqrt{2}V_\mathrm{mains}}, \tag{10}$$

where V_mains is the RMS value of the mains-phase voltage. A possible reactive current is rather small and has been neglected. With the mains frequency $f_\mathrm{mains} = 50\,\mathrm{Hz}$, losses, volume, and temperature of L_1 can be calculated.

The current in L_2 has a fundamental (sinusoidal) component, with an amplitude as calculated in (10) and a fundamental frequency of $f_\mathrm{mains} = 50\,\mathrm{Hz}$, and a superimposed
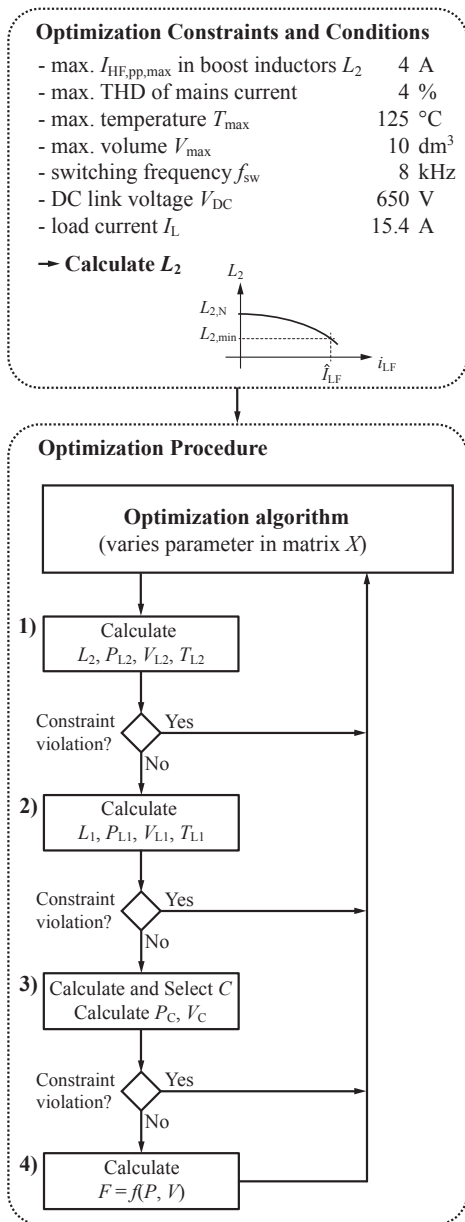
Fig. 6. The design procedure for three-phase LCL filters based on a generic optimization approach.

ripple current. The ripple current is, for simplification reasons, in a first step considered to be sinusoidal with constant amplitude $I_{\mathrm{HF,pp,max}}$ over the mains period. The losses for the fundamental and the high-frequency ripple are calculated independently, and then summed up. By doing this, it is neglected that core losses depend on the DC bias condition.

The ripple current is assumed to be fully absorbed by the filter capacitor C, hence, with the given dissipation factor $\tan\delta$, the losses in the capacitor can be calculated as well.

D. Optimization Procedure

After the optimization constraints and the simplifications chosen for the loss calculation have been described, the optimization procedure itself will be explained next.

A filter design is defined by

$$\mathbf{X} = \begin{pmatrix} a_{L_1} & a_{L_2} \\ w_{L_1} & w_{L_2} \\ N_{L_1} & N_{L_2} \\ do_{L_1} & do_{L_2} \\ h_{L_1} & h_{L_2} \\ t_{L_1} & t_{L_2} \\ ww_{L_1} & ww_{L_2} \\ d_{L_1} & d_{L_2} \end{pmatrix}, \qquad (11)$$

where all inductor parameters are defined as in Fig. 1(b). The subscripts L_1 and L_2 describe to which inductor each parameter corresponds. The capacitance value of the filter capacitor is calculated based on the L_1 value to guarantee that the THD constraint is met. The parameters in X are varied by an optimization algorithm to obtain the optimal design. The optimization is based on the MATLAB function `fminsearch()` that applies the Downhill-Simplex-Approach of Nelder and Mead [17].

The optimization algorithm determines the optimal parameter values in X. A design is optimal when the cost function

$$F = k_{\mathrm{Loss}} \cdot q_{\mathrm{Loss}} \cdot P + k_{\mathrm{Volume}} \cdot q_{\mathrm{Volume}} \cdot V, \qquad (12)$$

is minimized. k_{Loss}, k_{Volume} are weighting factors, q_{Loss}, q_{Volume} are proportionality factors, and P, V are the filter losses and filter volume, respectively. The proportionality factors are chosen such that, for a "comparable performance", $q_{\mathrm{Loss}} \cdot P$ and $q_{\mathrm{Volume}} \cdot V$ are in the same range[2]. In the case hand, this was achieved with $q_{\mathrm{Loss}} = 1/\mathrm{W}$ and $q_{\mathrm{Volume}} = 3 \cdot 10^4/\mathrm{m}^3$.

The following steps are conducted to derive the filter loss P and the filter volume V of (12) (cf. Fig. 6):

1) Calculate the inductance value L_2 as a function of the current. Furthermore, the losses P_{L_2}, the volume V_{L_2}, and temperature T_{L_2} of the boost inductors L_2 are calculated. In case a constraint cannot be met, the calculation is aborted and the design is discarded and a new design will be evaluated.

2) Calculate the inductance value L_1 as a function of the current. Furthermore, the losses P_{L_1}, the volume V_{L_1}, and temperature T_{L_1} of the filter inductors L_1 are calculated. In case a constraint cannot be met, the calculation is aborted and the design is discarded and a new design will be evaluated.

3) For simplification reasons, the THD without filter is approximated with $\mathrm{THD} = I_{\mathrm{HF,pp,max}}/I_{(1),\mathrm{pp}}$, where $I_{(1),\mathrm{pp}}$ is the fundamental peak-to-peak value of the

---

[2]The filter losses are in the range of approximately $100\,\mathrm{W} \ldots 250\,\mathrm{W}$, whereas the filter volumes are in the range of approximately $0.001\,\mathrm{m}^3 \ldots 0.01\,\mathrm{m}^3$. With $q_{\mathrm{Loss}} = 1/\mathrm{W}$ and $q_{\mathrm{Volume}} = 3 \cdot 10^4/\mathrm{m}^3$, the volume range is lifted to $30 \ldots 300$ and therewith becomes comparable to the losses.
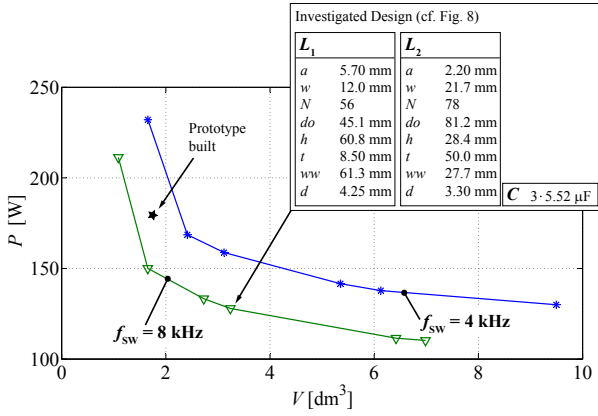
Fig. 7. Filter volumes V and filter losses P of different optimal designs.

Investigated Design (cf. Fig. 8)			
L_1		**L_2**	
a	5.70 mm	a	2.20 mm
w	12.0 mm	w	21.7 mm
N	56	N	78
do	45.1 mm	do	81.2 mm
h	60.8 mm	h	28.4 mm
t	8.50 mm	t	50.0 mm
ww	61.3 mm	ww	27.7 mm
d	4.25 mm	d	3.30 mm

C 3·5.52 µF

THD = 3.97 %
$P_{\text{Loss}} = 2.23$ W (simplified calculations: 1.65 W)

(a)

$I_{\text{HF,pp,max}} = \sim 4.1$ A
$P_{\text{Loss}} = 27.3$ W (simplified calculations: 34.7 W)

(b)
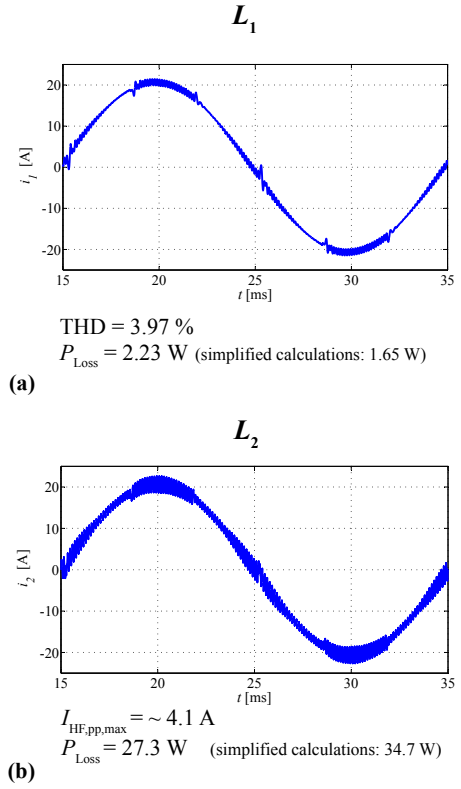
Fig. 8. Simulations and calculations to one selected design (cf. Fig. 7): (a) filter inductor $L_{1,a}$, (b) boost inductor $L_{2,a}$.

mains current[3]. Furthermore, it is assumed that the dominant harmonic content appears at f_{sw} (this assumption is motivated by simulation results). The LC-filter has then to attenuate the ripple current by $A = 20 \log_{10} \left(I_{(1),\text{pp}} \text{THD}_{\text{max}}/I_{\text{HF,pp,max}} \right)$ (in dB) at a frequency of f_{sw}. Therewith, C is calculated as

$$C = \frac{1}{L_1 \omega_0^2} = \frac{1}{L_1 (2\pi f_{\text{sw}} \cdot 10^{\frac{A}{40\,\text{dB}}})^2}, \qquad (13)$$

where ω_0 is the filter cutoff frequency. The losses and the volume of the capacitors and damping resistors can then be calculated. In case a constraint cannot be met, the calculation is aborted and the design is discarded and a new design will be evaluated.

4) The volume, temperature, and losses are now known and the cost function (12) can be evaluated.

The optimal matrix X is found by varying the matrix parameters, evaluating these designs by repeating above steps, and minimizing the cost function (12). After the optimal design is found, the algorithm quits the loop of Fig. 6.

V. OPTIMIZATION OUTCOMES

The optimization procedure leads to different filter designs depending on the chosen weighting factors k_1 and k_2 in (12), i.e. depending whether the aim of the optimization is more on reducing the volume V or more on reducing the losses P. Limiting factors are the maximum temperature T_{max} (limits the volume to become very small) and a maximum volume V_{max} (limits the efficiency to become very high). Different designs are shown by a P-V-plot, i.e. a P-V-Pareto front in Fig. 7; the trade-off between losses and volume can be clearly identified.

One design of Fig. 7 has been selected for further investigations. Particularly, a comparison between the (for the

---

[3]The THD is defined as $\text{THD} = \frac{\sqrt{I_2^2 + I_3^3 + I_4^4 + \cdots + I_n^n}}{I_1}$, where I_n is the RMS value of the nth harmonic and I_1 is the RMS value of the fundamental current. Under the assumption that only the dominant harmonic content $I_{\text{HF,pp,max}}$ (which for simplification reason is assumed to appear at one frequency) leads to a harmonic distortion, the THD becomes $I_{\text{HF,pp,max}}/I_{(1),\text{pp}}$, consequently.

optimization procedure) simplified and the more elaborate calculation based on voltage / current waveforms from a circuit simulator have been made. The filter parameters of the selected design are detailed in Fig. 7. The circuit of the three-phase PFC rectifier with the selected input filter has been simulated in MATLAB/Simulink, and the simulated current and voltage waveforms have been taken to calculate the losses according to Section III. The results are given in Fig. 8. The THD constraint is met and the current $I_{\text{HF,pp,max}}$ is only insignificantly higher. The simplified loss calculation used for the optimization leads to an overestimation of the boost inductor losses. This is due to the fact that the maximum ripple current has been assumed to be constant over the mains period. The losses in the filter inductors, on the other hand, have been underestimated as any high frequency ripple in the current through L_1 has been neglected in the simplified calculations. One could try to improve/change the simplifications made for the optimization and therewith improve the simplified loss calculation. However, the difference between the two calculation approaches has been considered as acceptable for this work; furthermore, with a slight overestimation of the losses one is always on the safe side.

Another important design criteria is the achieved power factor. The reactive power consumption of the the PFC rectifier system, including the damped LC input filter, is in the case at hand rather small (power factor = $\frac{\text{real power}}{\text{apparent power}} = 0.998$).

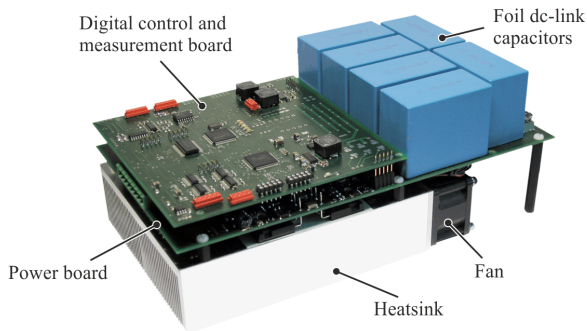So far all results are based on simulations and calculations.

Fig. 9. Photo of the PFC converter.

The models have to be verified experimentally to proof the validity of the optimization procedure. In the following section experimental results are shown.

VI. EXPERIMENTAL RESULTS

Experimental measurements have been conducted to show that the above introduced simulations / calculations are valid. The prototype built in the course of this work has been assembled of standard laminated sheets and standard coil formers to keep the cost low. This however avoids an exact implementation of the optimum as can be seen in Fig. 7. However, this does not impair the significance of the measurement results. Specifications, dimensions and photos of the LCL filter built are given in Fig. 10. All measurements have been carried out with a Yokogawa WT3000 Precision Power Analyzer.

The measurements have been conducted with the T-type converter introduced in [18]. In Fig. 9 a photo of the converter is given. The T-type converter is a 3-level converter, however, a 2-level operation is possible as well. A 2-level operation with the same modulation scheme (optimal-loss clamping modulation scheme) as in the MATLAB simulation has been implemented.

The results of the comparative measurements and simulations are given in Fig. 11 and Fig. 12. As can be seen, the calculated and measured loss values are very close to each other. The maximum current ripple in the actual system is (slightly) higher than in the simulation. This can be explained by the fact that in the simulation the inductance of the boost inductor is assumed to be constant over the full frequency range. However, in reality the effective inductance decreases with increasing frequency due to inductor losses and parasitic capacitances. The higher THD value can also be explained with the same effect as the filter inductance decreases with increasing frequency as well. The frequency behavior could be modeled by representing the inductors as RLC networks.

VII. CONCLUSION AND FUTURE WORK

A design procedure for three-phase LCL filters based on a generic optimization approach is introduced guaranteeing low volume and/or low losses. The cost function, which characterizes a given filter design, allows a weighting of the filter losses and of the filter volume according to the designer needs. Different designs have been calculated to show the

trade-off between filter volume and filter losses. Experimental results have shown that a very high loss accuracy has been achieved. To improve the THD and current ripple accuracy the frequency behavior of the inductors could be modeled as well.

An overall system optimization, i.e. an optimization of the complete three-phase PFC rectifier including the filter, could be performed by allowing selected optimization constraints to vary. For this work, the optimization has been conducted for different switching frequencies. As can be seen in Fig. 7, a higher switching frequency leads to lower volume, or, when
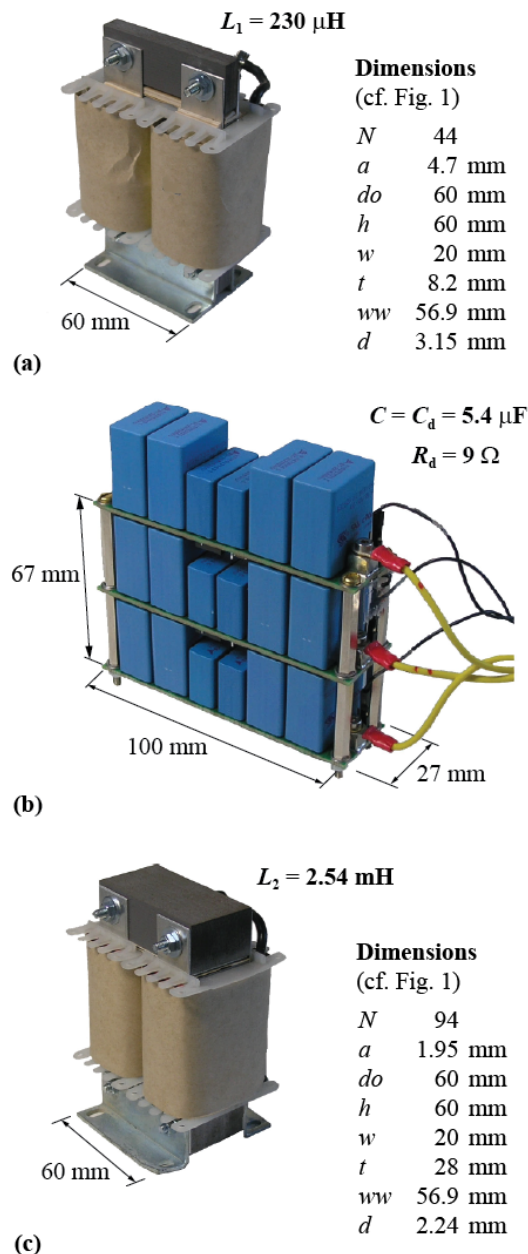

Fig. 10. Specifications, dimensions and photos of (a) one filter inductor L_1, (b) all filter and damping capacitors/resistors C, C_d and R_d, and (c) one boost inductor L_2.
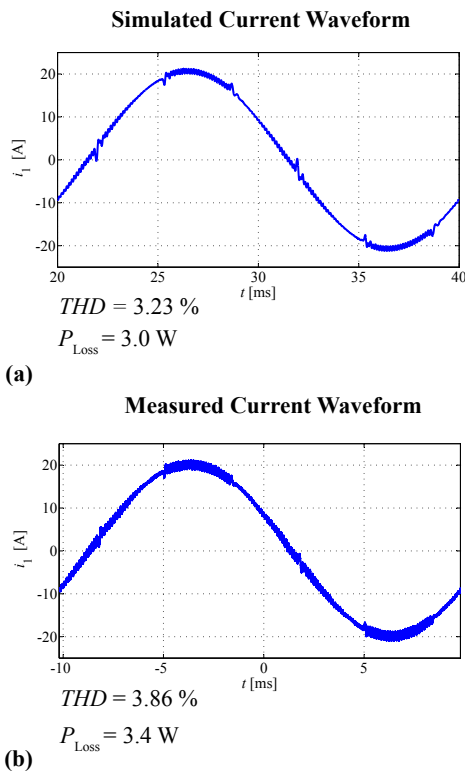
Simulated Current Waveform

$THD = 3.23\ \%$

$P_{\text{Loss}} = 3.0\ \text{W}$

(a)

Measured Current Waveform

$THD = 3.86\ \%$

$P_{\text{Loss}} = 3.4\ \text{W}$

(b)

Fig. 11. (a) Simulations and (b) measurements on one of the filter inductors L_1 of the implemented design.

Simulated Current Waveform

$I_{\text{HF,pp,max}} = 4.1\ \text{A}$

$P_{\text{Loss}} = 43.3\ \text{W}$

(a)

Measured Current Waveform

$I_{\text{HF,pp,max}} = 4.7\ \text{A}$

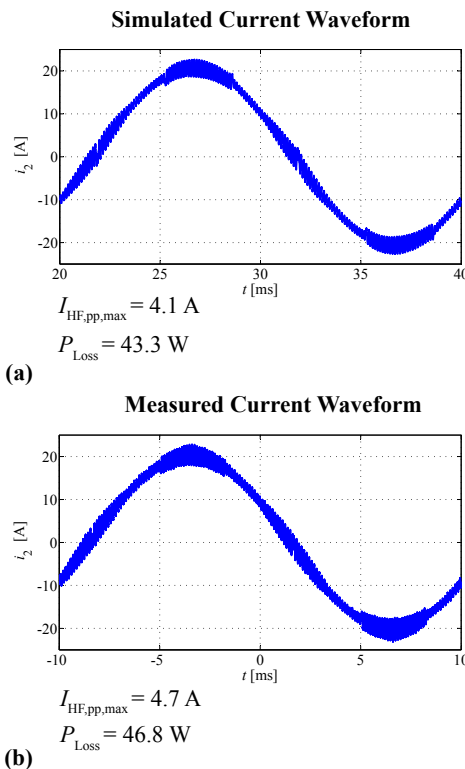$P_{\text{Loss}} = 46.8\ \text{W}$

(b)

Fig. 12. (a) Simulations and (b) measurements on one of the boost inductors of the implemented design.

keeping the volume constant, to lower losses. However, higher switching losses are expected in case of higher switching frequencies. Therefore, an overall system optimization including the power converter and / or the power semiconductors would be interesting in order to determine the overall optimum. In this case, other constraints are the maximum semiconductor junction temperature T_j and the maximum semiconductor area of the IGBT switches.

ACKNOWLEDGEMENT

REFERENCES

[1] J. W. Kolar, J. Biela, S. Waffler, T. Friedli, and U. Badstuebner, "Performance trends and limitations of power electronic systems," in *Proc. of the 6th International Conference on Integrated Power Electronics Systems (CIPS)*, pp. 1–20, 2010.

[2] M. Liserre, F. Blaabjerg, and S. Hansen, "Design and control of an LCL-filter-based three-phase active rectifier," *IEEE Transactions on Industry Applications*, vol. 41, pp. 1281–1291, 2005.

[3] S. V. Araujo, A. Engler, B. Sahan, and F. Antunes, "LCL filter design for grid-connected NPC inverters in offshore wind turbines," in *Proc. of the 7th Internatonal Conf. Power Electronics ICPE*, pp. 1133–1138, 2007.

[4] T. Friedli, *Comparative Evaluation of Three-Phase Si and SiC AC-AC Converter Systems*. PhD thesis, ETH Zurich, 2010.

[5] J. Mühlethaler, J. W. Kolar, and A. Ecklebe, "Loss modeling of inductive components employed in power electronic systems," in *Proc. of the 8th International Conference on Power Electronics - ECCE Asia*, pp. 945–952, 2011.

[6] J. Mühlethaler, J. W. Kolar, and A. Ecklebe, "A novel approach for 3D air gap reluctance calculations," in *Proc. of the 8th International Conference on Power Electronics - ECCE Asia*, pp. 446–452, 2011.

[7] J. Mühlethaler, J. Biela, J. W. Kolar, and A. Ecklebe, "Improved core loss calculation for magnetic components employed in power electronic systems," in *Proc. of Applied Power Electronics Conference and Exposition (APEC)*, 2011.

[8] J. Mühlethaler, J. Biela, J. W. Kolar, and A. Ecklebe, "Core losses under DC bias condition based on Steinmetz parameters," in *Proc. of the IEEE/IEEJ International Power Electronics Conference (ECCE Asia)*, pp. 2430–2437, 2010.

[9] J. Lammeraner and M. Stafl, *Eddy Currents*. Iliffe Books Ltd., 1966.

[10] L. C. Andrews, *Elementary Partial Differential Equations with Boundary Value Problems*. Academic Press College Division, 1986.

[11] P. Dowell, "Effects of eddy currents in transformer windings," *Proceedings of the Institution of Electrical Engineers*, vol. 113, no. 8, pp. 1387–1394, 1966.

[12] A. V. den Bossche and V. C. Valchev, *Inductors and Transformers for Power Electronics*. CRC Press, Taylor & Francis Group, 2005.

[13] *VDI Heat Atlas*. Springer-Verlag Berlin Heidelberg, 2010.

[14] *Film Capacitors, Edition 2009*. EPCOS AG.

[15] R. D. Middlebrook, "Design techniques for preventing input filter oscillations in switched-mode regulators," in *Proc. of Powercon 5*, pp. A3.1–A3.16, 1978.

[16] R. W. Erickson and D. Maksimovic, *Fundamentals of Power Electronics*. Springer Science+Business Media, LLC, 2004.

[17] J. A. Nelder and R. Mead, "A simplex method for function minimization," *The Computer Journal*, vol. 4, pp. 308–313, 1965.

[18] M. Schweizer and J. W. Kolar, "High efficiency drive system with 3-level t-type inverter," in *Proceedings of the 14th European Conference on Power Electronics and Applications - ECCE Europe, August 30 - September 1, 2011, Birmingham, UK*, 2011.